Damage Assessment Using the Auto-Correlation-Function-Based Damage Index

Muyu Zhang

Faculty of Civil Engineering and Mechanics, Jiangsu University, Zhenjiang, Jiangsu 212013, China.
Institute of Structural Health Management, Jiangsu University, Zhenjiang, Jiangsu 212013, China.
E-mail: muyu@ujs.edu.cn

Yujia Li, Xiaoyang Peng and Ziping Wang

Faculty of Civil Engineering and Mechanics, Jiangsu University, Zhenjiang, Jiangsu 212013, China.

Jianguo Zhu

Institute of Structural Health Management, Jiangsu University, Zhenjiang, Jiangsu 212013, China.

(Received 22 September 2022; accepted 28 June 2023)

A damage index describing damage severity based on the Auto correlation function at Maximum point value Vector (AMV) is proposed for damage assessment as well as locating the damage is described in this study. The detectability of the AMV-based damage detection method is compared with Mean Strain Energy (MSE) and the Generalized Flexibility Matrix (GFM) method, to show its efficiency in localizing the damage and its simplicity to conduct the analysis. Moreover, a procedure to estimate the damage severity using the sensitivity analysis is introduced. The stiffness reduction detection of a twelve-story shear frame structure is provided to show that the estimated damage severity by the AMV-based method is in close agreement with the simulated damage for small damage even when the measurement noise exists or is just part of the available modal parameters.

1. INTRODUCTION

Structural damage detection technique is one of the most important issues in structural health monitoring (SHM).[1,2] Over the last few decades, a wealth of research has been conducted in the vibration-based damage detection field for it requires no finite element model for the structure and can be performed in real-time/online.[3] The basic premise of the vibration-based damage detection methods is that the dynamic characteristics of the structure (natural frequency, mode shape, modal damping, etc.) will change when the physical parameters (mass, stiffness, etc.) of the structure change due to the damage. One can detect the changes of physical parameters using the changes of the dynamic parameters, such that the damage can be detected. A wide range of algorithms, methodologies and techniques have been developed for various problems and significant advancement has been achieved up to date.[4,5]

Damage sensitive features such as using natural frequency,[6,7] mode shape,[8,9] strain energy,[10,11] modal flexibility,[12–15] transmissibility,[16] etc., have been used to detect the damages in various structures under diverse situations. Dewangan et.al[10] proposed a damage index using modal strain energy for damage detection, with which they used their methodology on planetary gear train and parallel gear that gives promising results. Instead of using mode shape, Choi and Stubbs[11] used the vibration time-series response to derive the damage index, so called Mean Strain Energy (MSE). A beam structure simulation demonstrates that the MSE-based damage detection method can effectively locate and evaluate the damage with the existence of noise. While Wickramasinghe et.al[12] proposed a vertical damage index and lateral damage index based on the modal flexibility, with which the damage in Ölfusá suspension bridges can be located. Li et.al[13] used the decomposition of proportional flexibility matrix to locate the damage, which can decrease the influence of incomplete measured DOFs on structural damage detection under ambient excitation. Li and Wu[14] proposed the Generalized Flexibility Matrix (GFM) for damage detection to reduce the effect of truncating higher order. Peng and Yang[15] improved the Generalized Flexibility Method which used arbitrary-scaled mode shapes instead of mass-normalized mode shapes in the calculation.

Using the time-series response, the auto/cross correlation function becomes a viable tool in vibration-based damage detection.[17–29] Gradzki et.al[20] proposed a rotor fault detection approach by using auto-correlation and power spectral density. Both a numerical and experimental test of the rotor verified high sensitivity and reliability of the method. Lei and Xia[21] proposed an approach that combined the cross-correlation function of structural responses and the extended Kalman filter (EKF) to identify the damage under both independent stationary and non-stationary white noise excitations. Several numerical simulations and experimental studies of multi-story shear structure showed this method is validated for the structure under ambient excitation and is not sensitive to measurement noise. Wang and Chen[22] showed that the data fusion of the correlation function among different types of vibration measurements could significantly improve the accuracy of the identification. Hamidian and Soofi[23] proposed an output-only damage classification method using correlation function and information entropy, which has 93.98% accuracy for the test data. Taking the idea of Cross Correlation Function

Amplitude Vector (CorV)[24] and Inner Product Vector (IPV),[25] based on the theory of natural excitation technique (NExT),[26] Zhang and Schmidt[27–29] proposed the Auto correlation function at Maximum point value Vector (AMV) using the auto correlation function. Sensitivity analysis shows the normalized AMV has a sharp change around the local stiffness change area when damage appears, which can clearly indicate the location of the damage. Stiffness reduction detection of a 12-story shear frame structure compares the detectability of the AMV obtained from different response types (displacement, velocity and acceleration) under different excitations and measurement noises.

Rytter[30] categorized damage assessment into four levels: (1) damage presence identification; (2) damage localization; (3) damage severity quantification; and (4) remaining service life prediction. Normally, a wealth of papers just focus on detecting and locating the damage; that is, the first two levels of the damage assessment. This study is an extension of the Zhang and Schmidt paper[28] to not only locate the damage but also assess the damage severity. First, the theory of the AMV and sensitivity analysis is briefly reviewed. Second, an AMV-based damage location index is compared with MSE- and GFM-based damage location index for stiffness reduction detection of a 12-story shear frame structure. Then, damage severity is estimated by the theory from sensitivity analysis. Estimation results from a comparison of MSE- and GFM-based method, without/with measurement noise and from complete/incomplete modal parameter information are presented. Finally, conclusions are made.

2. DAMAGE INDEX

2.1. Auto Correlation Function at Maximum Point Value Vector

In this subsection, a brief derivation of the AMV introduced by Zhang and Schmidt[28] is presented. A standard matrix equation of motion for a given structure is expressed as:

$$\mathbf{M}\ddot{\mathbf{x}}(t) + \mathbf{C}\dot{\mathbf{x}}(t) + \mathbf{K}\mathbf{x}(t) = \mathbf{f}(t); \tag{1}$$

where $\mathbf{M}$ is the mass matrix, $\mathbf{C}$ is the damping matrix, $\mathbf{K}$ is the stiffness matrix, $\mathbf{f}$ is a vector of the force and $\mathbf{x}(t)$, $\dot{\mathbf{x}}(t)$ and $\ddot{\mathbf{x}}(t)$ is the vector of displacement, velocity and acceleration, respectively.

Suppose proportional damping $\mathbf{C} = \alpha\mathbf{M} + \beta\mathbf{K}$ and real normal modes are assumed, the displacement response $x_i(t)$ at point i due to input f_e at point e can be expressed by:

$$x_i(t) = \sum_{r=1}^{n} \phi_{ir}\phi_{er} \cdot \int_{-\infty}^{t} f_e(\tau) g^r(t-\tau) d\tau; \tag{2}$$

where ϕ_{ir}, ϕ_{er} is the ith and eth component of mode shape $\boldsymbol{\phi}_r$, respectively. And the function:

$$g^r(t) = \begin{cases} (1/m^r\omega_d^r) e^{-\zeta^r\omega_n^r t}\sin(\omega_d^r t) & t \geq 0 \\ 0 & t < 0 \end{cases}; \tag{3}$$

where m^r is the rth modal mass, ω_n^r is the rth modal frequency, $\zeta^r = (\alpha/\omega_n^r + \beta\omega_n^r)/2$ is the rth modal damping ratio, $\omega_d^r = \omega_n^r\sqrt{[1-(\zeta^r)^2]}$ is the damped modal frequency.

The auto correlation function of the vibration response $x_i(t)$ is defined as:

$$R_i(T) = E[x_i(t+T)x_i(t)]. \tag{4}$$

Substitute the expression of the vibration response in Eq. (2) into Eq. (4)

$$R_i(T) = \sum_{r=1}^{n}\sum_{s=1}^{n} \phi_{ir}\phi_{er}\phi_{js}\phi_{es} \cdot \int_{-\infty}^{t}\int_{-\infty}^{t+T} g^r(t+T-\sigma) g^s(t-\tau) E[f_e(\sigma)f_e(\tau)] d\sigma d\tau; \tag{5}$$

where the superscript r and s is the modal order.

Assume the excitation f_e is white noise, then the auto correlation function of this f_e can be expressed as:[31]

$$R_{f_e f_e}(\tau - \sigma) = E[f_e(\tau)f_e(\sigma)] = \varepsilon_e \delta(\tau - \sigma); \tag{6}$$

where ε_e is a constant representing the one-side auto-spectral density of white noise and $\delta(t)$ is the Dirac delta function.

Then, Eq. (5) can be further written by collapsing its first integration as:

$$R_i(T) = \sum_{r=1}^{n}\sum_{s=1}^{n} \varepsilon_e\phi_{ir}\phi_{er}\phi_{js}\phi_{es} \cdot \int_{-\infty}^{t} g^r(t+T-\tau) g^s(t-\tau) d\tau. \tag{7}$$

Assume $\lambda = t - \tau$, the limits of the integration in Eq. (7) can be changed to 0 and ∞, Eq. (7) can be further simplified as:

$$R_i(T) = \sum_{r=1}^{n}\sum_{s=1}^{n} \varepsilon_e\phi_{ir}\phi_{er}\phi_{js}\phi_{es} \cdot \int_{0}^{\infty} g^r(\lambda+T) g^s(\lambda) d\lambda. \tag{8}$$

Substitute the expression of the function $g(t)$ in Eq. (3) into Eq. (8) result in the auto correlation function of the vibration response $x_i(t)$ when the time lag $T = 0$ as:

$$R_i(0) = \sum_{r=1}^{n} \phi_{ir} \left[\sum_{s=1}^{n} \phi_{is}\mu_{rs}\right]; \tag{9}$$

where μ_{rs} is expressed as:

$$\mu_{rs} = \frac{2\varepsilon_e\phi_{er}\phi_{es}}{m^r m^s} \cdot \frac{\zeta^r\omega_n^r + \zeta^s\omega_n^s}{[(\omega_d^s+\omega_d^r)^2 + (\zeta^r\omega_n^r + \zeta^s\omega_n^s)^2] \cdot [(\omega_d^s-\omega_d^r)^2 + (\zeta^r\omega_n^r + \zeta^s\omega_n^s)^2]}. \tag{10}$$

An AMV vector is formed from the maximum value of the auto correlation function of the vibration response at different measurement locations, expressed as:

$$\mathbf{R} = [R_1, R_2, \ldots, R_n]^T. \tag{11}$$

Substituting Eq. (9) into Eq. (11), AMV can be written in matrix form as:

$$\mathbf{R} = \begin{bmatrix} \sum_{r=1}^{n}\sum_{s=1}^{n} \mu_{rs}\cdot(\phi_{1r}\phi_{1s}) \\ \sum_{r=1}^{n}\sum_{s=1}^{n} \mu_{rs}\cdot(\phi_{2r}\phi_{2s}) \\ \vdots \\ \sum_{r=1}^{n}\sum_{s=1}^{n} \mu_{rs}\cdot(\phi_{nr}\phi_{ns}) \end{bmatrix} = \sum_{r=1}^{n}\sum_{s=1}^{n} \mu_{rs}\cdot(\boldsymbol{\phi}_r \circ \boldsymbol{\phi}_s); \tag{12}$$

where '$\circ$' is the Hadamard product[32] symbol, then $\mathbf{R}$ can be considered as a weighted sum of the Hadamard product of two mode shape vectors.

In order to eliminate the influence of the constant ε_e that is related to the excitation, $\mathbf{R}$ is normalized by its root mean square value as follows:

$$\overline{\mathbf{R}} = \frac{\mathbf{R}}{rms(\mathbf{R})} = [\overline{R}_1, \overline{R}_2, \ldots, \overline{R}_n]^T; \tag{13}$$

where $rms(\mathbf{R}) = \sqrt{\frac{1}{n}\sum_{i=1}^{n} R_i^2}$.

Consequently, the damage index of the AMV method can be defined as:

$$\mathbf{D} = [D_1, D_2, \ldots, D_n]^T; \tag{14}$$

where D_i is the relative change of ith element in $\overline{\mathbf{R}}$ before and after damage, as:

$$D_i = \frac{\overline{R}_i^d - \overline{R}_i^u}{\overline{R}_i^u}; \tag{15}$$

where the superscript d denotes the damaged structural state and u is the healthy structural state.

The vector $\mathbf{D}$ defined in Zhang and Schmidt study[27,28] has a shape of 'step change',[25] thus in order to identify this damage location, a damage location index is defined as:

$$\mathbf{L} = [L_1, L_2, \ldots, L_{n-1}]^T; \tag{16}$$

where L_i is the difference of D_i, as:

$$L_i = D_i - D_{i-1}; \tag{17}$$

where the local maxima of $\mathbf{L}$ corresponding to the sudden change of the damage index of D_i. This sudden change is due to the change of the health state of the structure, i.e., damage occurs. Thus, the damage location can be identified.

2.2. Sensitivity Analysis

In the engineering arena, sensitivity analysis has been widely used to evaluate the change of one variable to the other, which can increase the understanding of the relationships between these two variables in the system.[33,34] One way to define the sensitivity is by the relative change of variable x to variable y, expressed as:

$$\eta(x/y) = \lim_{\Delta y \to 0} \frac{\Delta x/x}{\Delta y/y} = \frac{y}{x}\frac{\partial x}{\partial y}. \tag{18}$$

The sensitivity of the normalized AMV $\overline{\mathbf{R}}$ in Eq. (13) to the local stiffness k_j change is defined as:

$$\eta(\overline{\mathbf{R}}/k_j) = [\eta(\overline{R}_1/k_j), \eta(\overline{R}_2/k_j), \ldots, \eta(\overline{R}_n/k_j)]^T; \tag{19}$$

where the ith element is expressed as:

$$\eta(\overline{R}_i/k_j) = \frac{k_j}{\overline{R}_i}\frac{\partial \overline{R}_i}{\partial k_j}; \tag{20}$$

using the definition of the sensitivity in Eq. (18), where $\overline{R}_i$ is the ith element in the vector $\overline{\mathbf{R}}$ in Eq. (13).

Substitute Eq. (13) into the Hadamard product of $\eta(\overline{R}_i/k_j)$ and $\overline{\mathbf{R}}$ result in:

$$\eta(\overline{\mathbf{R}}/k_j) \circ \overline{\mathbf{R}} = \begin{bmatrix} \eta(\overline{R}_1/k_j) \\ \eta(\overline{R}_2/k_j) \\ \vdots \\ \eta(\overline{R}_n/k_j) \end{bmatrix} \circ \begin{bmatrix} \overline{R}_1 \\ \overline{R}_2 \\ \vdots \\ \overline{R}_n \end{bmatrix} = \begin{bmatrix} k_j \frac{\partial \overline{R}_1}{\partial k_j} \\ k_j \frac{\partial \overline{R}_2}{\partial k_j} \\ \vdots \\ k_j \frac{\partial \overline{R}_i}{\partial k_j} \end{bmatrix} = k_j \frac{\partial \overline{\mathbf{R}}}{\partial k_j}. \tag{21}$$

Using the definition of $\overline{\mathbf{R}}$ in Eq. (13) and note

$$\frac{\partial[rms(\mathbf{R})]}{\partial k_j} = \frac{1}{n}\frac{1}{rms(\mathbf{R})}\left(\mathbf{R}^T \cdot \frac{\partial \mathbf{R}}{\partial k_j}\right); \tag{22}$$

Eq. (21) can be rewritten as:

$$\eta(\overline{\mathbf{R}}/k_j) \circ \mathbf{R} = \left\{[1]_{n\times n} - \frac{1}{n}\overline{\mathbf{R}}\overline{\mathbf{R}}^T\right\} k_j \frac{\partial \mathbf{R}}{\partial k_j}; \tag{23}$$

where $[1]_{m\times n}$ is the $m \times n$ matrix that each element is 1. Define the sensitivity of μ_{rs} to the local stiffness k_j as:

$$\eta(\mu_{rs}/k_j) = \frac{k_j}{\mu_{rs}}\frac{\partial \mu_{rs}}{\partial k_j}; \tag{24}$$

and the sensitivity of the Hadamard product of mode shape $\boldsymbol{\Phi}_r \circ \boldsymbol{\Phi}_s$ to the local stiffness k_j as:

$$\eta[(\boldsymbol{\Phi}_r \circ \boldsymbol{\Phi}_s)/k_j] = [\eta(\phi_{1r}\phi_{1s}/k_j), \eta(\phi_{2r}\phi_{2s}/k_j), \ldots, \eta(\phi_{nr}\phi_{ns}/k_j)]^T. \tag{25}$$

Using the definition of the sensitivity in Eq. (18), the ith element of $\eta[(\boldsymbol{\Phi}_r \circ \boldsymbol{\Phi}_s)/k_j]$ can be expressed as:

$$\eta(\phi_{ir}\phi_{is}/k_j) = \frac{k_j}{\phi_{ir}\phi_{is}}\frac{\partial(\phi_{ir}\phi_{is})}{\partial k_j} = \frac{k_j}{\phi_{ir}\phi_{is}}\left(\frac{\partial \phi_{ir}}{\partial k_j}\phi_{is} + \phi_{ir}\frac{\partial \phi_{is}}{\partial k_j}\right). \tag{26}$$

Using the definition of $\overline{\mathbf{R}}$ in Eq. (13), and note Eq. (24) and Eq. (25), Eq. (23) result in:

$$\eta(\overline{\mathbf{R}}/k_j) \circ \mathbf{R} = \left\{[1]_{n\times n} - \frac{1}{n}\overline{\mathbf{R}}\overline{\mathbf{R}}^T\right\} \sum_{r=1}^{n}\sum_{s=1}^{n} \mu_{rs}\boldsymbol{\Phi}_r \circ \boldsymbol{\Phi}_s \circ \left\{\eta[(\boldsymbol{\Phi}_r \circ \boldsymbol{\Phi}_s)/k_j] + \eta[\mu_{rs}/k_j]\cdot[1]_{n\times 1}\right\}. \tag{27}$$

As a result, sensitivity of the normalized AMV to the local stiffness can be expressed by:

$$\eta(\overline{\mathbf{R}}/k_j) = \boldsymbol{\Theta}\sum_{r=1}^{n}\sum_{s=1}^{n} \mu_{rs}\boldsymbol{\Phi}_r \circ \boldsymbol{\Phi}_s \circ \left\{\eta[(\boldsymbol{\Phi}_r \circ \boldsymbol{\Phi}_s)/k_j] + \eta[\mu_{rs}/k_j]\cdot[1]_{n\times 1}\right\}; \tag{28}$$

where $\mathbf{\Theta} = \left\{\mathbf{R}^{\circ(-1)} \otimes [1]_{1\times n}\right\} \circ \left\{[1]_{n\times n} - \frac{1}{n}\overline{\mathbf{R}}\,\overline{\mathbf{R}}^T\right\}$, $\mathbf{R}^{\circ(-1)}$ is the Hadamard inverse[35] of $\mathbf{R}$, '$\otimes$' is the Kronecker product symbol.

From expression of the sensitivity of normalized AMV to the local stiffness in Eq. (28), the sensitivity of the modal parameters (frequency and mode shape) to the local stiffness is required, which can be obtained by Eq. (24) and Eq. (25). As from Eq. (24) and Eq. (25), these two sensitivities are both determined by the partial derivative of the modal parameters (frequency and mode shape) to the local stiffness.

For a given structure, the partial derivative of frequency ω_n^r to the local stiffness k_j is expressed by:[36]

$$\frac{\partial \omega_n^r}{\partial k_j} = \frac{1}{2\omega_n^r}\mathbf{\Phi}_r^T\left(\frac{\partial \mathbf{K}}{\partial k_j} - (\omega_n^r)^2\frac{\partial \mathbf{M}}{\partial k_j}\right)\mathbf{\Phi}_r; \tag{29}$$

and the partial derivative of mode shape $\mathbf{\Phi}_r$ to the local stiffness k_j is expressed by:

$$\frac{\partial \mathbf{\Phi}_r}{\partial k_j} = \sum_{i=1}^{n}\alpha_i\mathbf{\Phi_i}; \tag{30}$$

where:

$$\alpha_s = \begin{cases} \frac{1}{[(\omega_n^r)^2-(\omega_n^s)^2]}\mathbf{\Phi}_s^T\left(\frac{\partial \mathbf{K}}{\partial k_j} - (\omega_n^r)^2\frac{\partial \mathbf{M}}{\partial k_j}\right)\mathbf{\Phi}_r, & s \neq r; \\ -\frac{1}{2}\mathbf{\Phi}_r^T\frac{\partial \mathbf{M}}{\partial k_j}\mathbf{\Phi}_r, & s = r. \end{cases} \tag{31}$$

As the small damage is assumed that the mass will not change for the damage occurs, $\frac{\partial \mathbf{M}}{\partial k_j} = 0$. Thus,

$$\frac{\partial \omega_n^r}{\partial k_j} = \frac{1}{2\omega_n^r}\mathbf{\Phi}_r^T\left(\frac{\partial \mathbf{K}}{\partial k_j}\right)\mathbf{\Phi}_r; \tag{32}$$

$$\frac{\partial \mathbf{\Phi}_r}{\partial k_j} = \sum_{i=1}^{n}\alpha_i\mathbf{\Phi_i}; \tag{33}$$

where:

$$\alpha_s = \begin{cases} \frac{1}{[(\omega_n^r)^2-(\omega_n^s)^2]}\mathbf{\Phi}_s^T\left(\frac{\partial \mathbf{K}}{\partial k_j}\right)\mathbf{\Phi}_r, & s \neq r; \\ 0, & s = r. \end{cases} \tag{34}$$

From Eq. (32) and Eq. (33), the partial derivative of the modal parameters (frequency and mode shape) to the local stiffness are determined by the modal parameters and the partial derivative of the stiffness matrix to the local stiffness $\frac{\partial \mathbf{K}}{\partial k_j}$. As a result, the sensitivity of the normalized AMV to the local stiffness, the value of $\eta(\overline{\mathbf{R}}/k_j)$ in Eq. (28) can be obtained using the modal parameters and the partial derivative of the stiffness matrix to the local stiffness $\frac{\partial \mathbf{K}}{\partial k_j}$.

3. DAMAGE LOCALIZATION

A 12-story shear frame structure, as shown in Fig. 1, is used as a numerical simulation model to study the detectability of the AMV. It is assumed that the mass of each story is centralized on its floor and the stiffness of each floor is supplied by the braces between them. The stiffness in z direction is assumed to be much larger than the stiffness in x direction, such that the movement in x direction only needs to be considered.

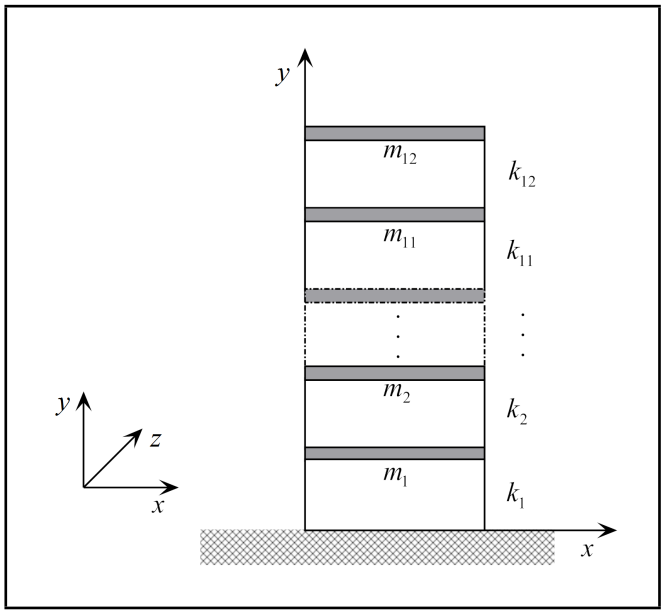

Figure 1. A 12-story shear frame structure.

Therefore, this shear frame structure can be expressed as a 12-DOF discrete system with the mass matrix:

$$\mathbf{M} = \mathsf{diag}[m_1, m_2, \ldots, m_{11}, m_{12}]; \tag{35}$$

and the stiffness matrix:

$$\mathbf{K} = \begin{bmatrix} k_1+k_2 & -k_2 & & & & \\ -k_2 & k_2+k_3 & -k_3 & & & \\ & \ddots & \ddots & \ddots & & \\ & & -k_{11} & k_{11}+k_{12} & -k_{12} \\ & & & -k_{12} & k_{12} \end{bmatrix}. \tag{36}$$

For each floor, the mass m_i is 1 kg and the stiffness coefficient k_i is 20,000 N/m. The mass proportional damping coefficient α is 0.002 and the stiffness proportional damping coefficient β is 0.001. As the mass matrix and the stiffness matrix are known, the 12th natural frequency of the structure can be easily obtained as 44.66 Hz. As the white noise that covers all the natural frequencies of the structure is used to deduce the expression of auto correlation function of the response in Eq. (9), $0 \sim 50$ Hz white noise that also covers all the natural frequencies is used as the excitation in this paper. The excitation force has a duration of 16 s with the sample frequency as 1,024 Hz and the magnitude is 1 N that is applied on the top of the structure, as shown in Fig. 1.

The stiffness coefficient k_i of the 2nd, 5th, 8th and 11th floor is reduced by 5% as the simulated damage, respectively. The displacement responses for the pristine and damaged structure respectively can be obtained using the Wilson-θ method with $\theta = 1.42$. After the responses are known, the AMV-based damage index and the corresponding damage location index can be obtained using Eq. (14) and Eq. (16), respectively.

The AMV-based damage location index is shown as the red solid lines in Fig. 2. For comparison, as both uses the vibration response, the damage detection results using the MSE-based method[11] are also plotted as blue dotted lines in Fig. 2. The MSE-based damage location index $\mathbf{L}_{MSE} =$

$[L_{MSE,1}, L_{MSE,2}, \ldots, L_{MSE,n}]^T$ is expressed as:

$$L_{MSE,i} \approx \frac{\sum_{q=1}^{NT} \mathbf{V}_q^T \mathbf{K} \mathbf{V}_q}{\sum_{q=1}^{NT} (\mathbf{V}_q^d)^T \mathbf{K} \mathbf{V}_q^d} \cdot \left(\frac{\sum_{q=1}^{NT} (\mathbf{V}_q^d)^T \mathbf{G}_i \mathbf{V}_q^d + \sum_{q=1}^{NT} (\mathbf{V}_q^d)^T \mathbf{K} \mathbf{V}_q^d}{\sum_{q=1}^{NT} \mathbf{V}_q^T \mathbf{G}_i \mathbf{V}_q + \sum_{q=1}^{NT} \mathbf{V}_q^T \mathbf{K} \mathbf{V}_q} \right); \quad (37)$$

where i is the measurement location, $\mathbf{V}_q = \mathbf{V}(t_q) = [v_1(t_q), v_2(t_q), \ldots, v_n(t_q)]^T$ is the displacement response vector with $v_i(t_q)$ is the displacement response at measurement location i of time t_q, $\mathbf{K}$ is the stiffness matrix of the intact structure, $\mathbf{G}_i$ is the geometric portion of the contribution for the ith element to the stiffness matrix of the structure and NT is the number of sampling points. The superscript d denotes the parameter is from the damaged structure.

Additionally, as the flexibility matrix is very popular to formulate the damage indicator, the GFM-based[15] damage location index $\mathbf{L}_{GFM} = [L_{GFM,1}, L_{GFM,2}, \ldots, L_{GFM,n}]^T$ is also used for comparison. It is obtained by solving the linear equations

$$\sum_{i=1}^{n} L_{GFM,i} (\mathbf{F}^u \mathbf{K}_{ui} \mathbf{F}^u \mathbf{M} \mathbf{F}^u + \mathbf{F}^u \mathbf{M} \mathbf{F}^u \mathbf{K}_{ui} \mathbf{F}^u) = \sum_{z=1}^{mo} \frac{1}{(\omega_d^z)^4} \mathbf{\Phi}_z^d (\mathbf{\Phi}_z^d)^T - \sum_{z=1}^{mo} \frac{1}{(\omega_n^z)^4} \mathbf{\Phi}_z^u (\mathbf{\Phi}_z^u)^T; \quad (38)$$

using the least squares method, where $\mathbf{F}$ is the flexibility matrix, $\mathbf{K}_{ui}$ is the ith element stiffness matrix, $\mathbf{M}$ is the mass matrix, mo is the number of measured modes (in this paper it is chosen as 1), $\mathbf{\Phi}_z$ is the zth mode shape vector, u and d denote the parameter is from the intact and damaged structure, respectively.

The GFM-based damage location index is plotted as green dash-dotted lines in Fig. 2. As the exact value of the AMV-, MSE- and GFM-based damage location index is different, in order for comparison all the damage location indexes are normalized by

$$\bar{\mathbf{L}} = \frac{\mathbf{L} - E(\mathbf{L})}{\sigma(\mathbf{L})}; \quad (39)$$

where $E(\mathbf{L})$ and $\sigma(\mathbf{L})$ is the expectation and standard deviation value of the corresponding damage location index, respectively.

As shown in Fig. 2, AMV-, MSE- and GFM-based damage location index have the similar trend and shape. In Fig. 2(a), the AMV-based damage location index has a peak value at floor number 2, which indicates the damage lies in the 2nd floor according to Eq. (16). Similarly, the detected damage lies in the 5th, 8th and 11th floor in Fig. 2(b), Fig. 2(c) and Fig. 2(d), respectively, which is exactly the damage location simulated. On the other hand, MSE- and GFM-based damage detection method also has the peak value of the damage location index at floor number 2, 5, 8 and 11, which indicates the damage also lies in the 2nd, 5th, 8th and 11th floor, respectively.

As a result, both AMV-, MSE- and GFM-based damage location index can locate the damage correctly. It is worth noting that in order to get the MSE-based damage location index, the stiffness matrix $\mathbf{K}$ of the structure is required as shown in Eq. (38), and in order to get the GFM-based damage location index, the element stiffness matrix $\mathbf{K}_{ui}$ and mass matrix $\mathbf{M}$ are required as shown in Eq. (39), which none is easily obtained in real applications. However, for the AMV-based damage location index, only the displacement response is needed. The AMV-based damage detection method has the advantage of simplicity in calculation and a similar detectability as the MSE- and GFM-based damage detection method.

4. DAMAGE ASSESSMENT (SEVERITY)

4.1. Damage Severity Estimation

Figure 3 is the AMV-based damage location index change with the stiffness reduction from 0 to 10% with an interval of 1% for the 2nd, 5th, 8th and 11th floor, respectively. From these subfigures, the damage location is clearly identified by the peak value location of the damage location index. And as the stiffness reduction increases, this peak value also increases. As the other values do not change much, this peak value is a clear indicator for the damage severity. If this damage location index is monitored, after checking the peak value of it, the relative change of the damage severity can be observed. Same phenomenon is found for the MSE- and GFM-based damage location index that the peak value of the damage location index increases when the damage becomes severe.

On the other hand, with just monitoring the AMV-based damage location index, the exact value of damage severity and stiffness reduction could not be obtained. In real applications, one needs to find the damage as early as possible.[37] If the damage is assumed to be very small, the sensitivity of the normalized AMV to the local stiffness can be expressed as:

$$\eta(\overline{\mathbf{R}}/k_j) = \frac{\Delta \overline{\mathbf{R}}/\overline{\mathbf{R}}}{\Delta k_j/k_j}. \quad (40)$$

Thus, the relative change of the local stiffness prior to and after damage occurs in the structure can be estimated by:

$$\Delta k_j/k_j = \frac{1}{n} \left[\sum_{i=1}^{n} \frac{\Delta \overline{\mathbf{R}}_i/\overline{\mathbf{R}}_i}{\eta(\overline{\mathbf{R}}_i/k_j)} \right] = \frac{1}{n} \left[\sum_{i=1}^{n} \frac{D_i}{\eta(\overline{\mathbf{R}}_i/k_j)} \right]. \quad (41)$$

For a given structure, the partial derivative of the frequency and mode shape to the local stiffness can be obtained when the mass matrix and the stiffness matrix are available or using the modal testing technique in real application, then the value of $\eta(\overline{\mathbf{R}}/k_j)$ can be obtained using Eq. (28). The value of D_i can be calculated using the displacement response before and after damage using Eq. (15). Then, the stiffness reduction can be estimated using Eq. (41).

The 12-story shear frame structure in Fig. 1 is again taken as an example. The damage is still simulated by stiffness reduction in the 2nd, 5th, 8th and 11th floor from 0 to 10%, respectively. The corresponding displacement response is obtained using the Wilson-θ method. The estimated stiffness reduction is shown in Tables 1–4 for these cases using Eq. (41). In comparison, the estimated severity from the MSE and the GFM-based damage detection methods are calculated based on the results from Eq. (37) and Eq. (38) and also shown in Tables 1–4, respectively. Moreover, the measurement noises are added

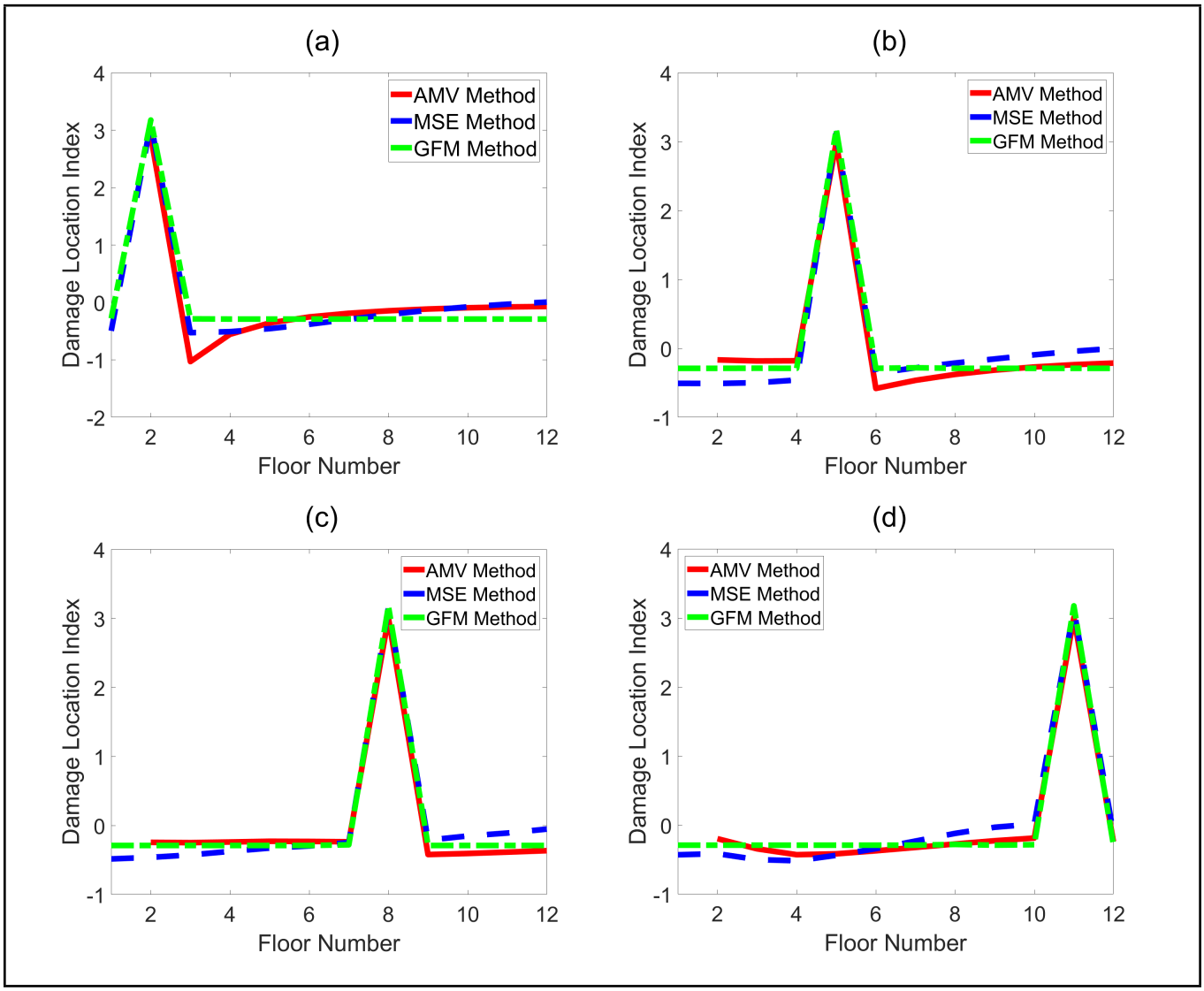

Figure 2. Comparison of the damage detection results. Damage occurs in (a) 2nd floor; (b) 5th floor; (c) 8th floor; and (d) 11th floor.

to the response signals for different cases, the mean value of estimated stiffness reduction by the AMV-based method from 200 cases is also shown in Tables 1–4.

Table 1 shows the estimated stiffness loss for the case when the damage is in the 2nd floor. The 1st column is the simulated stiffness loss from 0 to 10% with an interval of 1%. The 2nd, 5th and 6th column is the estimated stiffness loss using AMV-, MSE- and GFM-based method when there is no noise, respectively. The 2nd and 3rd column is the estimated stiffness loss obtained from the AMV-based method when the response signal is contaminated with 20 dB and 10 dB measurement noise, respectively. Comparing these results, the value in the 2nd column is very close to the value in the 1st column. The estimated stiffness loss from the AMV-based method is very close to the simulated stiffness loss. On the other hand, the value in the 2nd and 3rd column is also close to the value in the 1st column, which means the estimated stiffness loss from the AMV-based method with the noise exists, even when the measurement noise is as high as 10 dB, it is still close to the simulated stiffness loss. Additionally, comparing the values in 2nd and 5th column with the values in 1st column, the estimated stiffness loss from AMV-based method is closer to the simulated stiffness loss than the MSE-based method. While

Table 1. Estimation of stiffness reduction when damage occurs in the 2nd floor.

Simulated	Estimated				
	AMV			MSE	GFM
	No noise	$SNR = 20$ dB	$SNR = 10$ dB	No noise	No noise
0	0	-0.0026	-0.0019	0	0
0.01	0.0122	0.0146	0.0002	0.0129	0.0099
0.02	0.0248	0.0258	0.0192	0.0261	0.0195
0.03	0.0378	0.0387	0.0440	0.0396	0.0290
0.04	0.0511	0.0518	0.0459	0.0534	0.0382
0.05	0.0649	0.0633	0.0716	0.0675	0.0471
0.06	0.0791	0.0799	0.0816	0.0818	0.0559
0.07	0.0937	0.0942	0.0928	0.0964	0.0644
0.08	0.1088	0.1089	0.1110	0.1113	0.0726
0.09	0.1243	0.1211	0.1300	0.1265	0.0807
0.10	0.1403	0.1394	0.1481	0.1418	0.0885

comparing the values in the 2nd and 6th column with the values in 1st column, the estimated stiffness loss from the GFM-based method is closer to the simulated stiffness loss than the AMV-based method. As a result, for the damage in the 2nd floor, the GFM-based method has the best estimation results; the AMV-based method comes in second; and, the MSE-based method comes in third.

Tables 2–4 show the estimation results for the case when the damage is in the 5th, 8th and 11th floor, respectively. Compar-

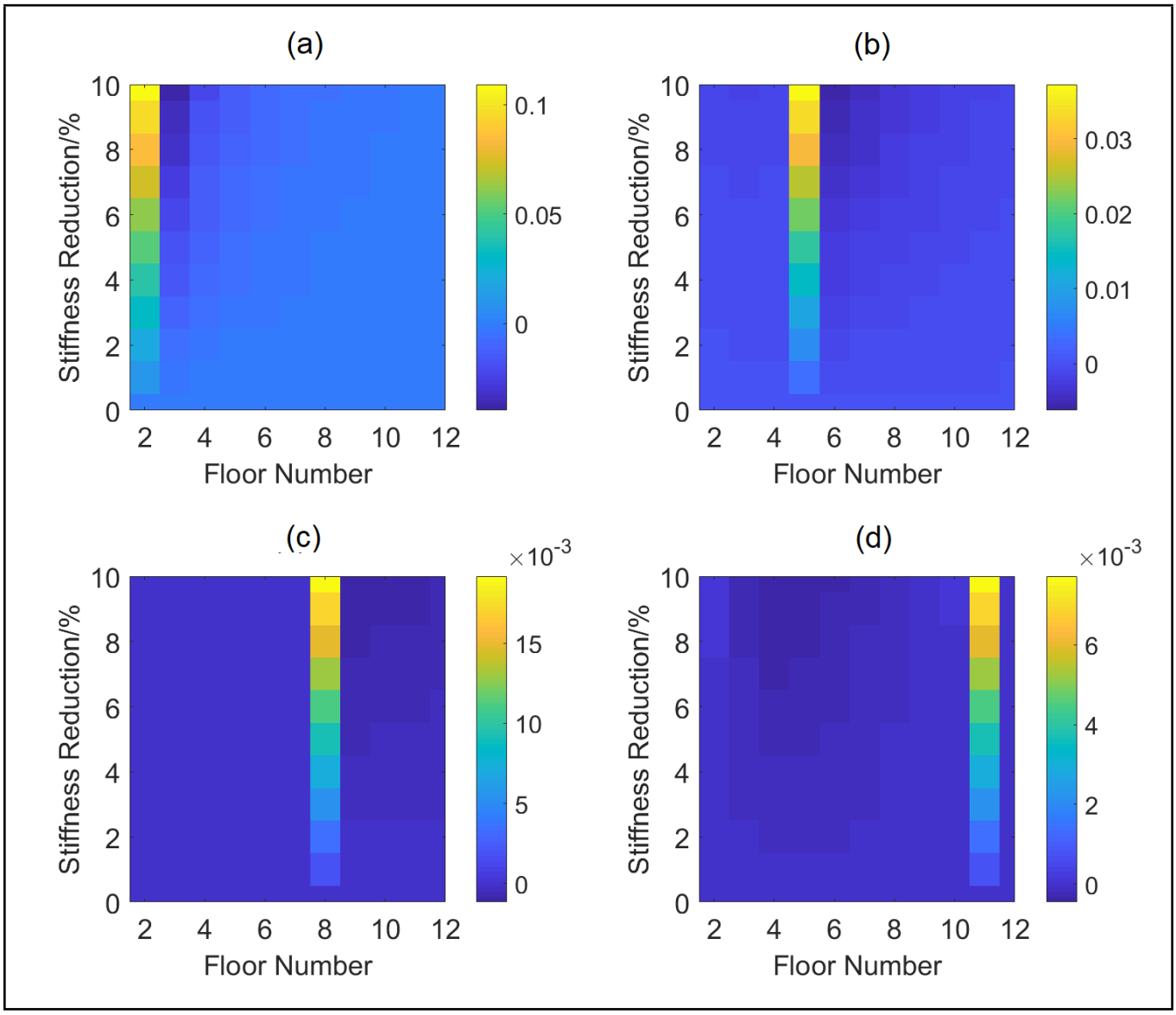

Figure 3. AMV-based damage location index change with damage severity.

Table 2. Estimation of stiffness reduction when damage occurs in the 5th floor.

Simulated	Estimated				
	AMV			MSE	GFM
	No noise	$SNR = 20$ dB	$SNR = 10$ dB	No noise	No noise
0	0	0.0009	0.0012	0	0
0.01	0.0127	0.0151	0.0151	0.0095	0.0099
0.02	0.0257	0.0269	0.0207	0.0192	0.0196
0.03	0.0388	0.0383	0.0320	0.0292	0.0290
0.04	0.0521	0.0536	0.0433	0.0394	0.0383
0.05	0.0655	0.0679	0.0592	0.0498	0.0473
0.06	0.0790	0.0817	0.0757	0.0604	0.0560
0.07	0.0927	0.0895	0.0910	0.0713	0.0646
0.08	0.1065	0.1051	0.1127	0.0824	0.0729
0.09	0.1203	0.1193	0.1194	0.0937	0.0810
0.10	0.1342	0.1346	0.1416	0.1053	0.0889

Table 3. Estimation of stiffness reduction when damage occurs in the 8th floor.

Simulated	Estimated				
	AMV			MSE	GFM
	No noise	$SNR = 20$ dB	$SNR = 10$ dB	No noise	No noise
0	0	0.0001	-0.0009	0	0
0.01	0.0089	0.0091	0.0091	0.0060	0.0099
0.02	0.0180	0.0176	0.0176	0.0121	0.0196
0.03	0.0273	0.0275	0.0275	0.0185	0.0290
0.04	0.0367	0.0365	0.0355	0.0250	0.0382
0.05	0.0464	0.0462	0.0491	0.0316	0.0473
0.06	0.0562	0.0558	0.0564	0.0385	0.0560
0.07	0.0663	0.0669	0.0652	0.0456	0.0646
0.08	0.0766	0.0765	0.0775	0.0528	0.0730
0.09	0.0871	0.0871	0.0863	0.0603	0.0811
0.10	0.0979	0.0975	0.0968	0.0680	0.0891

ing these values in different columns, the results are similar as Table 1 that the estimated stiffness loss from the AMV-based method is also very close to the simulated stiffness loss even when the measurement noises exist, which shows this AMV-based methodology has a very good noise tolerance to estimate the damage severity. Moreover, comparing these results in four tables, when the damage is smaller (same damage location, less stiffness reduction or same stiffness reduction, closer to the top of the structure), the relative error of the estimated and simulated stiffness loss is also smaller. That is because Eq. (41) is only valid and more accurate when the damage is very small. Therefore, this AMV-based damage severity estimation procedure is suitable for the small/early damage case.

Additionally, the estimation results of the MSE-based

Table 4. Estimation of stiffness reduction when damage occurs in the 11th floor.

Simulated	Estimated				
	AMV			MSE	GFM
	No noise	$SNR = 20$ dB	$SNR = 10$ dB	No noise	No noise
0	0	-0.0061	0.0088	0	0
0.01	0.0096	0.0081	0.0120	0.0021	0.0097
0.02	0.0196	0.0205	0.0247	0.0042	0.0193
0.03	0.0299	0.0332	0.0322	0.0064	0.0286
0.04	0.0405	0.0413	0.0426	0.0086	0.0377
0.05	0.0515	0.0517	0.0563	0.0110	0.0466
0.06	0.0629	0.0647	0.0688	0.0134	0.0553
0.07	0.0747	0.0761	0.0680	0.0158	0.0639
0.08	0.0870	0.0868	0.0903	0.0184	0.0721
0.09	0.0997	0.0998	0.1042	0.0210	0.0802
0.10	0.1129	0.1170	0.1174	0.0237	0.0881

method in Tables 1–4 were compared as the damage is close to the top of the structure, that is, the damage is smaller, the estimated stiffness loss is farther away from the simulated stiffness loss. While this is not the case for the GFM-based estimation results, it is nearly the same in these four tables in that it can estimate the stiffness loss very close to the simulated ones. On the other hand, when the damage is near the top of the structure, the estimated stiffness loss from the AMV-based method is closer to the simulated stiffness loss than the GFM-based method. As a result, when comparing these results among 2nd, 3rd and 4th columns, the AMV-based method has better estimation results than the MSE- and GFM-based methods especially for the real small damages.

4.2. Effect of The Modal Orders Considered

In the previous section, the damage severity can be well estimated by the AMV-based method using Eq. (41). Note that all the modal orders are considered in calculating the value of $\eta(\overline{\mathbf{R}}/k_j)$ in Eq. (28). But in real applications, it is rather difficult or sometimes even unlikely to get all modal parameters.

According to Eq. (9) and Eq. (28), the value of μ_{rs} is the weight to calculate the AMV and the sensitivity of the normalized AMV to the local stiffness. As the modal order r or/and s increase, the frequency ω_n^r or/and ω_n^s will increase, such that the value of μ_{rs} expressed in Eq. (10) will decrease. Figure 4 is the value of μ_{rs} calculated using Eq. (10) in this 12-story shear frame structure case, which shows it decreases rapidly when the modal order r or/and s increase. As a result, the value of $\eta(\overline{\mathbf{R}}/k_j)$ is dominated by the lower modal order of modal parameters from Eq. (28). Such that Eq. (28) can be rewritten as:

$$\eta(\overline{\mathbf{R}}/k_j) \approx \boldsymbol{\Theta} \sum_{r=1}^{p} \sum_{s=1}^{p} \left\{ \eta[(\boldsymbol{\Phi}_r \circ \boldsymbol{\Phi}_s)/k_j] + \eta[\mu_{rs}/k_j] \cdot [1]_{n\times 1} \right\} \circ \boldsymbol{\Phi}_r \circ \boldsymbol{\Phi}_s \cdot \mu_{rs}; \quad (42)$$

where p is the number of modes to be considered and $\boldsymbol{\Theta} = \left\{ \mathbf{R}^{\circ(-1)} \otimes [1]_{1\times n} \right\} \circ \left\{ [1]_{n\times n} - \frac{1}{n} \overline{\mathbf{R}} \overline{\mathbf{R}}^T \right\}$.

Table 5 shows the estimated stiffness loss when different modes are considered for computing the value of $\eta(\overline{\mathbf{R}}/k_j)$ when the damage is in the 11th floor with/without noise using the same procedure as in Section 4.1. The 2nd column is the estimated stiffness loss result that all the modal parameters

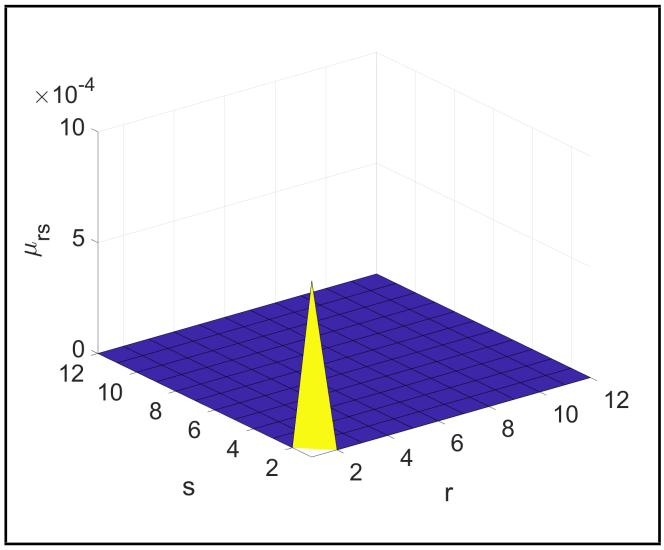

Figure 4. Value of μ_{rs}.

are considered. While in the 4th/5th, 6th/7th and 8th/9th columns, only the 1st, the first 2 and the first 5 modes are used to estimate the stiffness loss. As can be seen from Table 5, as more and more modes are used, the estimated results are much closer to the results for all the modes. But even when there is just the first mode information available and the response is contaminated with 10 dB noise, the damage severity can still be estimated accurately. Therefore, the AMV-based estimation procedure proposed in this paper is also suitable for the case when there is just a portion of the modal parameters.

5. CONCLUSIONS

An AMV-based damage detection method used in conjunction with sensitivity analysis is proposed to assess the damage severity besides determining the damage location. The method is compared to two popular methods: MSE method and GFM method. The simulation shows its advantage that it uses the vibration response to get the similar detectability to localize the damage compared to the MSE- and GFM-based methods. Note that in order to obtain the MSE-based damage location index, the stiffness matrix of the structure needs to be known *in priori*. In order to get the GFM-based damage location index, both the elemental stiffness matrix and mass matrix are required.

An estimation procedure based on a sensitivity analysis was used to estimate the damage severity of the structure. Several cases show that this AMV-based method has a better estimation result than the MES- and GFM-based method when the damage is very small. Moreover, even with a high noise level measurement noise, this methodology can still get the local stiffness reduction. When just a small part of the modal parameters is available, the estimated results are still capable of evaluating the damage severity of the structure. This method is well suited to the incipient local damage after it appears in the structure, which would be an effective alarm for early structural health monitoring.

Table 5. Estimation of stiffness reduction when different number of modes is used.

Simulated	Number of modes are considered							
	All modes		Only 1st mode		First 2 modes		First 5 modes	
	No noise	$SNR = 10$ dB	No noise	$SNR = 10$ dB	No noise	$SNR = 10$ dB	No noise	SNR=10 dB
0	0	0.0088	0	0.0032	0	-0.0010	0	-0.0098
0.01	0.0096	0.0120	0.0082	0.0021	0.0092	0.0136	0.0096	0.0041
0.02	0.0196	0.0247	0.0166	0.0179	0.0186	0.0273	0.0194	0.0108
0.03	0.0299	0.0322	0.0252	0.0287	0.0283	0.0330	0.0296	0.0229
0.04	0.0405	0.0426	0.0340	0.0290	0.0384	0.0351	0.0401	0.0377
0.05	0.0515	0.0563	0.0431	0.0505	0.0487	0.0576	0.0510	0.0432
0.06	0.0629	0.0688	0.0525	0.0534	0.0595	0.0628	0.0622	0.0558
0.07	0.0747	0.0680	0.0621	0.0673	0.0706	0.0673	0.0739	0.0655
0.08	0.0870	0.0903	0.0721	0.0714	0.0821	0.1010	0.0860	0.0962
0.09	0.0997	0.1042	0.0823	0.0884	0.0940	0.0905	0.0986	0.0999
0.10	0.1129	0.1174	0.0928	0.0951	0.1063	0.1114	0.1117	0.1096

ACKNOWLEDGEMENTS

The work was supported by the National Natural Science Foundation of China [Grant No. 11972014], the Natural Science Foundation of Jiangsu Province [Grant No. BK 20190834], and Research Start-up Foundation at Jiangsu University [Grant No. 19JDG027]

REFERENCES

[1] Zhang, C. W., Mousavi, A. A., Masri, S. F., Gholipour, G., Yan, K., and Li, X. L. Vibration feature extraction using signal processing techniques for structural health monitoring: A review, *Mechanical Systems and Signal Processing*, **177**, 109175, (2022). https://doi.org/10.1016/j.ymssp.2022.109175

[2] Singh, T. and Sehgal, S. Structural health monitoring of composite materials, *Archives of Computational Methods in Engineering*, **29**, 1997–2017, (2022). https://doi.org/10.1007/s11831-021-09666-8

[3] Hou, R. and Xia, Y. Review on the new development of vibration-based damage identification for civil engineering structures: 2010–2019, *Journal of Sound and Vibration*, **491**, 115741, (2021). https://doi.org/10.1016/j.jsv.2020.115741

[4] Toh, G. and Park, J. Review of vibration-based structural health monitoring using deep learning, *Applied Sciences*, **10** (5),1680, (2020). https://doi.org/10.3390/app10051680

[5] Gomes, G. F., Mendez, Y. A. D., Alexandrino, P. D. L., Cunha, S. S. D., and Ancelotti, A. C. A review of vibration based inverse methods for damage detection and identification in mechanical structures using optimization algorithms and ANN, *Archives of Computational Methods in Engineering*, **26** (4), 883-897, (2018). https://doi.org/10.1007/s11831-018-9273-4

[6] Pan, J. W., Zhang, Z. F., Wu, J. R., Ramakrishnan, K. R., and Singh, H. K. A novel method of vibration modes selection for improving accuracy of frequency-based damage detection, *Composites Part B: Engineering*, **159**, 437–446, (2019). https://doi.org/10.1016/j.compositesb.2018.08.134

[7] Dubey, A., Denis, V., and Serra, R. A novel VB-SHM strategy to identify geometrical damage properties using only frequency changes and damage library, *Applied Sciences*, **10** (23), 8717, (2020). https://doi.org/10.3390/app10238717

[8] Duvnjak, I., Damjanović, D., Bartolac, M., and Skender, A. Mode shape-based damage detection method (MSDI): experimental validation, *Applied Sciences* **11** (10), 4589, (2021). https://doi.org/10.3390/app11104589

[9] He, W. Y., He, J., and Ren, W. X. The use of mode shape estimated from a passing vehicle for structural damage localization and quantification, *International Journal of Structural Stability and Dynamics*, **19** (10), 1950124, (2019). https://doi.org/10.1142/S0219455419501244

[10] Dewangan, P., Parey, A., Hammami, A., Chaari, F., and Haddar, M. Damage detection in wind turbine gearbox using modal strain energy, *Engineering Failure Analysis*, **107**, 104228, (2020). https://doi.org/10.1016/j.engfailanal.2019.104228

[11] Choi, S. and Stubbs, N. Damage identification in structures using the time-domain response, *Journal of Sound and Vibration*, **275** (3–5), 577–590, (2004). https://doi.org/10.1016/j.jsv.2003.06.010

[12] Wickramasinghe, W. R., Thambiratnam, D. P., and Chan, T. H. T. Damage detection in a suspension bridge using modal flexibility method, *Engineering Failure Analysis*, **107**, 104194, (2020). https://doi.org/10.1016/j.engfailanal.2019.104194

[13] Li, G. Q., Luo, S., Su, R., Wang, Z. M., and Wang, C. Research on damage diagnosis based on flexibility matrix decomposition, *Applied Mathematics and Mechanics*, **42** (3), 292–298, (2021). https://doi.org/10.21656/1000-0887.410257

[14] Li, J., Wu, B. S., Zeng, Q. C., and Lim, C. W. A generalized flexibility matrix based approach for structural damage detection, *Journal of Sound and Vibration*, **329** (22), 4583–4587, (2010). https://doi.org/10.1016/j.jsv.2010.05.024

[15] Peng, X. and Yang, Q. W. Sensor placement and structural damage evaluation by improved generalized flexibility, *IEEE Sensors Journal*, **21** (10), 11654–11664, (2021). https://doi.org/10.1109/JSEN.2021.3066989

[16] Lei, Y., Zhang, Y. X., Mi, J. N., Liu, W. F., and Liu, L. J. Detecting structural damage under unknown

seismic excitation by deep convolutional neural network with wavelet-based transmissibility data, *Structural Health Monitoring*, **20** (4), 1583–1596, (2021). https://doi.org/10.1177/1475921720923081

[17] Chen, Y. C. Vibration-based structural damage localisation using time response correlation, *Nondestructive Testing and Evaluation*, **38** (1), 112–129, (2023). https://doi.org/10.1080/10589759.2022.2077938

[18] Li, W. and Huang, Y. A method for damage detection of a jacket platform under random wave excitations using cross correlation analysis and PCA-based method, *Ocean Engineering*, **214**, 107734, (2020). https://doi.org/10.1016/j.oceaneng.2020.107734

[19] Li, X. Y., Ye, X. Q., and Law, S. S. Damage identification with fusion of estimates from covariance of IRF in different frequency bands, *Mechanical Systems and Signal Processing*, **134**, 106327, (2019). https://doi.org/10.1016/j.ymssp.2019.106327

[20] Gradzki, R., Kulesza, Z., and Bartoszewicz, B. Method of shaft crack detection based on squared gain of vibration amplitude, *Nonlinear Dynamic*, **98** (1), 671–690, (2019). https://doi.org/10.1007/s11071-019-05221-0

[21] Lei, Y., Qiu, H., and Zhang, F. Identification of structural element mass and stiffness changes using partial acceleration responses of chain-like systems under ambient excitations, *Journal of Sound and Vibration*, **488**, 115678, (2020). https://doi.org/10.1016/j.jsv.2020.115678

[22] Wang, X. J., Chen, F., Zhou H. Y., Ni, P. H., Wang, L. H., and Zhang, J. Structural damage detection based on cross-correlation function with data fusion of various dynamic measurements, *Journal of Sound and Vibration*, **541**, 117373, (2022). https://doi.org/10.1016/j.jsv.2022.117373

[23] Hamidian, P., Soofi, Y. J., and Bitaraf, M. A comparative machine learning approach for entropy-based damage detection using output-only correlation signal, *Journal of Civil Structural Health Monitoring*, **12**, 975–990, (2022). https://doi.org/10.1007/s13349-022-00587-z

[24] Yang, Z. C., Yu, Z. F., and Sun, H. On the cross correlation function amplitude vector and its application to structural damage detection, *Mechanical Systems and Signal Processing*, **21**, 2918–2932, (2007). https://doi.org/10.1016/j.ymssp.2007.03.004

[25] Wang, L., Yang, Z. C., and Waters, T. P. Structural damage detection using cross correlation functions of vibration response, *Journal of Sound and Vibration*, **329**, 5070-5086, (2010). https://doi.org/10.1016/j.jsv.2010.06.020

[26] Farrar, C. R. and James III, G. H. System identification from ambient vibration measurements on a bridge, *Journal of Sound and Vibration*, **205** (1), 1–18, (1997). https://doi.org/10.1006/jsvi.1997.0977

[27] Zhang, M. and Schmidt, R. Sensitivity analysis of an auto-correlation-function-based damage index and its application in structural damage detection, *Journal of Sound and Vibration*, **333** (26), 7352–7363, (2014). https://doi.org/10.1016/j.jsv.2014.08.020

[28] Zhang, M. and Schmidt, R. Study on an auto-correlation-function-based damage index: Sensitivity analysis and structural damage detection, *Journal of Sound and Vibration*, **359**, 195–214, (2015). https://doi.org/10.1016/j.jsv.2015.09.004

[29] Zhang, M. and Schmidt, R. Numerical investigation of structural damage detection methods using the correlation function, *Journal of Vibration Engineering & Technologies*, **3** (2), 169–184, (2015).

[30] Rytter, A. *Vibrational Based Inspection of Civil Engineering Structures*, Aalborg University, Denmark, (1993).

[31] Bendat, J. S. and Piersol, A. *Random data: Analysis and Measurement Procedures*, 4th ed., J.Wiley, (2010).

[32] Styan, G. P. H. Hadamard products and multivariate statistical analysis, *Linear Algebra and its Applications*, **6**, 217–240, (1973). https://doi.org/10.1016/0024-3795(73)90023-2

[33] Saltelli, A., Ratto, M., and Andres, T. *Global Sensitivity Analysis: The Primer*, John Wiley & Sons, (2008).

[34] Saltelli, A. Sensitivity analysis for importance assessment, *Risk Analysis*, **22** (3), 579–590, (2010). https://doi.org/10.1111/0272-4332.00040

[35] Reams, R. Hadamard inverses, square roots and products of almost semidefinite matrices, *Linear Algebra and its Applications*, **288**, 35–43, (1999). https://doi.org/10.1016/S0024-3795(98)10162-3

[36] Zhao, J. and DeWolf, J. T. Sensitivity study for vibrational parameters using in damage detection, *Journal of Structural Engineering*, **125**, 410–416, (1999). https://doi.org/10.1061/(ASCE)0733-9445(1999)125:4(410)

[37] Parloo, E., Guillaume, P., and Overmeire, M. V. Damage assessment using mode shape sensitivities, *Mechanical Systems and Signal Processing*, **17** (3), 499–518, (2003). https://doi.org/10.1006/mssp.2001.1429